Dynamic charge susceptibility for the infinite-U Anderson model

T. Brunner and D. C. Langreth
Department of Physics and Astronomy, Rutgers University, Piscataway, New Jersey 08855-0849
(Received 23 May 1996)

The dynamic charge susceptibility for the single-impurity N-fold degenerate Anderson model is calculated within the noncrossing approximation. The calculations were done in all regimes: empty orbital, mixed valent, and Kondo. At large N in the Kondo regime the results can be connected at low temperatures with the predictions of large-N mean-field theory, suggesting a range of temperature where the validity of the two theories overlaps. Our smaller N results are presented in the context of electronic friction and energy transfer of an atom or molecule moving outside a metallic surface. It is suggested that some of the dramatic temperature and frequency dependences obtained should be relevant for this surface problem. [S0163-1829(97)00703-0]

I. INTRODUCTION

This study is motivated by a problem in surface physics. When a particle (atom or molecule, neutral or charged) interacts with a metal there may be both phonon and electron processes going on in the surface. Low-energy ($<$ eV) scattering of rare gases, for example, is dominated by phonon processes,[1,2] neutralization of high energy ($\approx$ keV) ions in scattering is obviously caused by electronic (charge exchange) processes.[3,4] Of course, there are cases where both mechanisms might contribute, for example vibrational damping[5–13] for CO on Cu and Pt or excitation of molecular vibration in scattering for NO/Ag.[14–17] In any case there is experimental evidence of nonadiabatic electronic coupling in a number of simple cases including desorption of adsorbed molecules,[18–20] damping of vibrational modes of molecule-surface systems,[20–22] and charge-transfer in ion-surface scattering and desorption experiments.[23–25] Recently, this role of electronic non-adiabaticity has been reemphasized through laser-induced desorption experiments and the accompanying theory.[26–28]

The usual way to describe charge-exchange processes in surface problems is by means of a time-dependent Anderson model.[29,30] Many treatments neglect spin and the intra-adsorbate Coulomb interaction U, but different improvements have been suggested.[31–33] Langreth and Nordlander developed a general and consistent solution of the time-dependent degenerate level problem with infinite U.[34] It is based on the so-called noncrossing approximation (NCA) (Refs. 35–39) for the stationary problem. This was earlier justified as an expansion in $1/N$ (N being the degeneracy of the electronic adsorbate level), although it is perhaps better regarded as a thermodynamically self-consistent and conserving approximation in its own right, which except at very low temperatures, which are not generally relevant for the surface problem, reproduces the correct features of the exact solution, including the Kondo and mixed valent states. Its accuracy has recently been studied in comparison with the exact numerical renormalization-group solution for $N=2$ at low temperatures.[40]

The NCA was generalized[34] to the nonequilibrium time-dependent situation using nonequilibrium double-time Green's-function techniques introduced by Kadanoff and Baym[41] and by Keldysh.[42] It was shown that the intra-adsorbate correlation can drastically change the charge-transfer dynamics. An exact numerical solution for the time-dependent Green's functions was given by Shao, Langreth, and Nordlander.[43] The procedure followed in the present paper, however, is simply to linearize the time-dependent NCA equations,[34] and then iterate them to self-consistency, thus obtaining the linear-response functions exactly within the NCA.

An eventual application might be to the damping or line shapes of adsorbate vibrations, in situations where the Kondo or correlated mixed-valent states could have anomalous effects. For example, NO/Cu(111) has been recently argued[44] to be a Kondo system on the basis of an experimental determination of the Anderson model parameters. Undoubtedly there exist many other such systems with equilibrium parameters in an interesting range. More generally, a practical scheme for molecular dynamics at surfaces in the presence of electronic dissipation has been developed[45] and successfully applied.[46] This scheme used friction coefficients, related to the charge susceptibilities calculated here, but neglecting the correlations induced by the intra-atomic Coulomb interaction considered here. In such problems one might expect to be in the range where such neglected correlations should be important in a large number of cases; as we see, the presence of these correlations can make a qualitative difference in the nature of the response.

In this paper we consider the response of the mean occupation of an atomic level to a shift in the level position, as would occur as the atomic species moved perpendicularly to a metal surface. The imaginary or dissipative part of this response is related to the electronic friction coefficient for a movement in this direction. Also related is the response to a change in the tunneling matrix element from the atomic level to the surface. As noted recently,[47,48] the interplay between these two responses can be important, at least when quantitative results are required. In addition, a level degeneracy $N=2$ or perhaps $N=4$, would be more common than the the $N=6$ results which, in order to simplify the numerical calculation, we present here. Nevertheless, these are quantitative, not qualitative considerations, which can be relieved by heavier numerical work when specific systems are under consideration. Here we simply calculate the charge suscepti-

bility for a model system, and demonstrate for the benefit of surface theoretical development the huge differences in temperature and frequency dependence that intra-atomic Coulomb correlations can make under the appropriate conditions, and more generally provide for both surface and bulk communities benchmark NCA charge susceptibility calculations that have not previously been performed, to our knowledge. Such results may also have application to quantum dots and similar resonant tunneling systems, which should be Kondo systems in appropriate parameter regimes.[49–55]

In the context of bulk problems, dynamic response for the infinite-U Anderson problem has been widely discussed (magnetic impurities). Kuramoto suggested a thermodynamically self-consistent formalism for general dynamic susceptibilities via a generating functional.[37] The formalism was applied for the dynamic *magnetic* susceptibility.[56] Müller-Hartmann discussed the $T=0$ limit of the formalism.[57] Spurious NCA results for low frequencies or low temperatures were examined.[58,59] Further studies — again on the dynamic *magnetic* susceptibility — were performed by Maekawa *et al.*[60] and by Bickers, Cox, and Wilkins;[61] see also the comprehensive review article by Bickers.[62] For a very recent and general review, see Hewson.[63]

Dynamic *charge* susceptibility has been explicitly discussed in two studies for the Kondo regime. Coleman[64] calculated magnetic and charge susceptibilities for arbitrary frequencies around $T=0$, within a mean-field theory which is valid in the limit $N=\infty$ provided that the filling factor is kept finite.[65] Though our calculation cannot be extended to $T=0$ we can study the temperature dependence for higher T. Coleman's study and ours cover opposite regions in temperature. We will refer to his results for the susceptibilities in detail. We will try to associate the numerical results which can be derived with his formulas for low temperatures and the results which we get for higher temperatures. The work by Jin and co-workers,[66] which presents qualitative arguments designed to cure the NCA's breakdown at very low temperatures, is also conceptually related to our study.

In the following we will present dynamic charge susceptibilities for a wide range of frequencies and temperatures for the Kondo regime, the mixed-valence regime, and the empty impurity regime. As we are mainly interested in dissipative nonadiabatic processes we will usually discuss the imaginary part of the susceptibility. For comparison we also show dynamic magnetic susceptibilities, which we do not claim to be shown for the first time, but a comparison facilitates the interpretation of our results. Finally we also show results for the single-level $U=0$ model (resonant level model) in order to emphasize the large effects the Coulomb interaction has on the charge response.

II. MODEL

A. Degenerate level

For describing the interaction between electrons on the degenerate electronic level of the adsorbate particle and conduction electrons in the metal, we consider the following time-dependent Anderson Hamiltonian

$$H=\sum_m \epsilon_m(t)n_m+U\sum_{m>m'} n_m n_{m'}+\sum_{km}\epsilon_k n_{km} + \frac{1}{\sqrt{N}}\sum_{km}(V_k c_{km}^\dagger c_m+\text{H.c.}), \tag{2.1}$$

where m enumerates the N states which would be degenerate due to an assumed symmetry in the absence of the small time-dependent perturbation, $\epsilon_m(t)$ is the time-dependent energy of the adsorbate electronic level, and $n_m=c_m^\dagger c_m$ is the number operator for the adsorbate level m. U is the Coulomb repulsion between electrons on the adsorbate level which causes the strong correlation. The quantity ϵ_k is the band energy of the metallic electrons, assumed to depend only on their other quantum numbers k, and not on m, and $n_{km}=c_{km}^\dagger c_{km}$ is the number operator for band electrons. V_k is the hopping matrix element between adsorbate states and conduction states (hybridization). We have included a prefactor $1/\sqrt{N}$; therefore it is not necessary to rescale V_k when studying the N dependence.

We take $\epsilon_n(t)$ to vary harmonically with

$$\epsilon_m(t)=\epsilon+\delta\epsilon_m(t)=\epsilon+\delta\epsilon_m(\Omega)\exp(-i\Omega t), \tag{2.2}$$

where $\delta\epsilon_m(t)$ is assumed to be small. Therefore the average occupancy of the mth orbital $\langle n_m\rangle(t)$ will take a similar form

$$\langle n_m\rangle(t)=\langle n_0\rangle+\delta\langle n_m\rangle(t)=\langle n_0\rangle+\delta\langle n_m\rangle(\Omega)\exp(-i\Omega t), \tag{2.3}$$

where $\langle n_0\rangle$ is defined to be the occupancy of *one* of the N atomic orbitals in the absence of the perturbation $\delta\epsilon_m(t)$. The susceptibility tensor is then defined by

$$\delta\langle n_m\rangle(\Omega)=-\sum_n \chi_{mn}(\Omega)\,\delta\epsilon_n(\Omega). \tag{2.4}$$

Generally one wants the response of a linear combination $\Sigma_m\alpha_m\delta\langle n_m\rangle$ to a specified combination of level shifts $\delta\epsilon_n=\alpha_n\delta\epsilon$. We take the set of coefficients $[\alpha]$ to be normalized such that

$$\sum_m \alpha_m^2=N. \tag{2.5}$$

For each set $[\alpha]$ we define a susceptibility

$$\chi_{[\alpha]}(\Omega)=\sum_{mn}\alpha_m\chi_{mn}(\Omega)\alpha_n. \tag{2.6}$$

For cases with simple symmetries, there are only two independent cases: (i) the charge susceptibility χ_{charge} where all the levels move together $[\alpha_n=1]$, and (ii) the magnetic susceptibility χ_{magn} where the mean position of the levels is unchanged $[\Sigma_n\alpha_n=0]$. The magnetic susceptibility, which is easy to calculate within the NCA and for which a number of studies already exist, is considered here for comparison and discussion.

Following Coleman[39] and Langreth and Nordlander,[34] we perform the infinite-U limit by adopting the slave-boson technique. The Hamiltonian is rewritten

$$H=\sum_m \epsilon_n(t)n_m+\sum_{km} \epsilon_k n_{km}+\frac{1}{\sqrt{N}}\sum_{km} (V_k c_{km}^\dagger b^\dagger c_m+\text{H.c.}); \tag{2.7}$$

it must be studied in the subspace where the number operator

$$Q=b^\dagger b+\sum_m n_m \tag{2.8}$$

has the eigenvalue 1.

B. Single level

As we are especially interested in the effect of the degeneracy and the intra-adsorbate Coulomb correlation, we compare all results with results for the nondegenerate model ($N=1$) or resonant level model or Fano-Anderson model, a variant of which has often been used in the surface charge-transfer problem. The Hamiltonian is

$$H=\epsilon(t)n+\sum_k \epsilon_k n_k+\sum_k (V_k c_k^\dagger c+\text{H.c.}). \tag{2.9}$$

Here $n=c^\dagger c$ is the number operator for the adsorbate level. For this case there is but a single ϵ and hence but a single susceptibility. Similarly if we were to increase N but keep $U=0$, the charge and magnetic susceptibilities would be equal to each other and larger by a factor of N.

C. Terminology

We take over the real-time Green's function terminology of Langreth and Nordlander,[34] using, for example, the notation $iG_m(t,t')$ for the adsorbate electron Green's function $\langle Tc_m(t)c_m^\dagger(t')\rangle$. We always assume a sufficient symmetry that the basis may be chosen so that it is diagonal in m. In fact we usually suppress the m subscripts altogether, because there is no m dependence in the charge susceptibility case $\alpha_m=1$. Similarly, the slave-boson Green's function is $iB(t,t')=\langle Tb(t)b^\dagger(t')\rangle$. According to conventions defined before,[67] we use retarded (G^R, B^R) and advanced (G^A, B^A) propagators, and less than ($G^<$, $B^<$) and greater than ($G^>$, $B^>$) propagators. Usually we write only equations for the retarded and less than quantities, advanced and greater than propagators fulfill similar equations.[34,43] As long as we have a time-dependent nonequilibrium problem there are two time arguments (t,t'); for an equilibrium problem propagators depend on the time difference $(t-t')$ only. Equilibrium quantities are marked by the subscript ''eq.'' In equilibrium the fermion spectral density, for example, is given by $-\text{Im}G_{\text{eq}}^R(\omega)/\pi=\text{Im}G_{\text{eq}}^A(\omega)/\pi$, the occupied fermion spectral density by $G_{\text{eq}}^<(\omega)/2\pi$, and the total adsorbate charge after integration over frequency by $NG_{\text{eq}}^<(t-t'=0)$. A more complete summary of our notation for the thermal equilibrium theory is given in Appendix A. G is the physical fermion propagator for the single-level case (where there is no B at all). For the degenerate level case the physical fermion propagator consists of a convolution of the auxiliary propagators G and B, as illustrated schematically in Fig. 1.

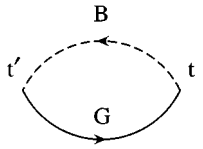

FIG. 1. Physical adsorbate electron propagator $A(t,t')$ in the NCA.

D. Conduction-band electrons

The dependence of the NCA equations on the band electrons can be expressed in terms of the the quantity K, whose retarded form is given in frequency space by

$$K^R(\omega)=\sum_k |V_k|^2\frac{1}{\omega-\epsilon_k+i\delta}, \tag{2.10}$$

while

$$K^<(\omega)=e^{-\beta\omega}K^>(\omega)=-2\,\text{Im}K^R(\omega)f(\omega), \tag{2.11}$$

where $f(\omega)=(\exp(\beta\omega)+1)^{-1}$. In particular,

$$-\text{Im}K^R(\omega)/\pi=\sum_k |V_k|^2\delta(\omega-\epsilon_k)=\langle|V|^2\rho\rangle(\omega), \tag{2.12}$$

where ρ is the band density of states. As previously, we take a simple parabolic form for $\langle|V|^2\rho\rangle$, such that

$$-\text{Im}K^R(\omega)=\begin{cases}\Delta[1-(\omega/D)^2], & |\omega|\leq D\\ 0, & |\omega|>D.\end{cases} \tag{2.13}$$

The real part is then given by a Kramers-Kronig relation

$$\text{Re}K^R(\omega)=\frac{\Delta}{\pi}\left[\frac{2\omega}{D}-\left(1-\frac{\omega^2}{D^2}\right)\ln\left|\frac{1-\omega/D}{1+\omega/D}\right|\right]. \tag{2.14}$$

For comparison with earlier papers,[34,43] one should notice that the width parameter Δ in this paper is the same as $N\Delta$ in the earlier papers due to the different definition of V in Eq. (2.7). All energies and temperatures in this paper are measured in units of the new Δ. Furthermore, in all our numerical calculations we take $D=5$ in these units.

E. Connection to vibrational damping and friction coefficients at a surface

Consider an adsorbate oscillating in some normal mode at the surface. The force $\delta F(\Omega)$ on the nucleus induced by the change in level position $\delta\epsilon(\Omega)$ will be

$$\delta F(\Omega)=-\frac{\partial\epsilon}{\partial Q}\delta\langle n\rangle(\Omega), \tag{2.15}$$

where Q is the appropriate nuclear normal coordinate. There will also be a force induced by the change in the magnitude and phase of V_k as the nucleus moves. The effect of varying the magnitude of V_k has been neglected in early work in the field,[5] although it has been suggested that in some situations the cooperative or cancelling effect of ϵ and Δ changes can be important when quantitative results are needed.[47] For motions parallel to the surface, where Δ and ϵ would vary only

due to deviations of the surface from planarity, the force due the change in phase of V_k is crucial. Thus the discussion here using only Eq. (2.15) is not applicable to the parallel motion case, and incomplete for the perpendicular motion case. Although the rectification of this deficiency is relatively simple, it involves other response functions than χ_{charge}, and so is more appropriately discussed in a separate publication.

Using χ_{charge} to express Eq. (2.15) in terms of the nuclear motion gives

$$\delta F(\Omega)=\left(\frac{\partial\epsilon}{\partial Q}\right)^2\chi_{\text{charge}}(\Omega)\,\delta Q(\Omega). \tag{2.16}$$

Inserting Eq. (2.16) into Newton's equation of motion gives the following equation for the (complex) Ω:

$$\Omega^2=\Omega_0^2-\frac{1}{M}\left(\frac{\partial\epsilon}{\partial Q}\right)^2\chi_{\text{charge}}(\Omega), \tag{2.17}$$

where M is the mass and Ω_0 is the mode frequency in the absence of level repopulation. Solution of Eq. (2.17) gives the shifted resonant frequency Ω and damping constant γ, the latter being minus twice imaginary part of the complex resonant frequency:

$$\gamma(\Omega)=\frac{1}{M}\left(\frac{\partial\epsilon}{\partial Q}\right)^2\frac{\text{Im}\chi_{\text{charge}}(\Omega)}{\Omega}, \tag{2.18}$$

where, to simplify the discussion, we have neglected the correction involving the frequency derivative of Reχ, which is usually negligible in any case.

The friction coefficient K is defined as the ratio of nuclear force to nuclear velocity in the slow limit, that is, $K=M\gamma(0)$. This is the limit in which vibrational damping is usually discussed, because normally one expects vibrational motion to be slow on the electronic time scale due to mass ratio arguments. It is also the limit used in molecular-dynamics theory of Head-Gordon and Tully.[45] In this limit one may use the Korringa-Shiba relation Eq. (B5) to express the friction coefficient in terms of the static response,

$$K=\pi\left(\frac{d\langle n\rangle}{dQ}\right)^2, \tag{2.19}$$

which can equivalently be written in terms of the phase shift δ through the Friedel rule[68] $\langle n\rangle=\delta/\pi$. Equation (2.19) is thus more general than its original derivations in the case of potential scattering,[69] or in the case of the $U=0$ Anderson model.[70,5]

However, we know that the presence of the Kondo or correlated mixed-valent state may provide a slow electronic time scale, which will necessitate keeping a finite frequency in Eq. (2.18). In addition, even for very slow nuclear motion, K may have anomalous temperature dependence because of the slow electronic time scales. The extent to which these effects should occur is one of the subjects of this paper.

III. GENERAL TIME-DEPENDENT SOLUTION

The general time-dependent generalization of the NCA was given by Langreth and Nordlander.[34] For the sake of completeness we repeat the integrodifferential equations given before. These equations are rewritten here in the form of integral equations, which can specify the deviation from equilibrium more explicitly. The general time-dependent solution, be it in the form of the integrodifferential equations or in the form of the integral equations, is the basis of our derivation of the linear response in Sec. IV.

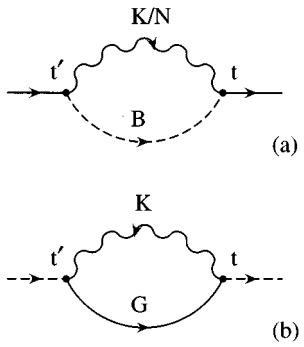

FIG. 2. Self-energies in the NCA: (a) $\Sigma(t,t')$ for the auxiliary fermion and (b) $\Pi(t,t')$ for the slave boson.

A. Degenerate level

The equations for the retarded propagators are the following:

$$[i\partial_t-\epsilon-\delta\epsilon_m(t)]G_m^R(t,t')$$

$$=\delta(t-t')+\int dt_1\Sigma^R(t,t_1)G_m^R(t_1,t'), \tag{3.1}$$

$$i\partial_t B^R(t,t')=\delta(t-t')+\int dt_1\Pi^R(t,t_1)B^R(t_1,t'). \tag{3.2}$$

The NCA expressions for the self-energies, as illustrated generically in Fig. 2, are specifically given for the retarded functions by

$$\Sigma^R(t,t')=\frac{1}{N}K^>(t-t')B^R(t,t') \tag{3.3}$$

and

$$\Pi^R(t,t')=\frac{1}{N}\sum_m K^<(t'-t)G_m^R(t,t'). \tag{3.4}$$

Using the equilibrium functions (see Appendix A), these equations can be transformed into the equivalent integral equations

$$G_m^R(t,t')=G_{\text{eq}}^R(t-t')+\int dt_1 G_{\text{eq}}^R(t-t_1)\int dt_2$$
$$\times[\delta\epsilon_m(t_1)\delta(t_1-t_2)+\Sigma^R(t_1,t_2)-\Sigma_{\text{eq}}^R(t_1-t_2)]$$
$$\times G_m^R(t_2,t') \tag{3.5}$$

and

$$B^R(t,t')=B^R_{\rm eq}(t-t')+\int dt_1 B^R_{\rm eq}(t-t_1)\int dt_2 \times[\Pi^R(t_1,t_2)-\Pi^R_{\rm eq}(t_1-t_2)]B^R(t_2,t'). \tag{3.6}$$

The equations for the lesser propagators are

$$[i\partial_t-\epsilon-\delta\epsilon_m(t)]G^<_m(t,t')=\int dt_1[\Sigma^R(t,t_1)G^<_m(t_1,t') +\Sigma^<(t,t_1)G^A_m(t_1,t')], \tag{3.7}$$

$$i\partial_t B^<(t,t')=\int dt_1[\Pi^R(t,t_1)B^<(t_1,t') +\Pi^<(t,t_1)B^A(t_1,t')], \tag{3.8}$$

where the self energies (see Fig. 2) are in this case given by

$$\Sigma^<(t,t')=\frac{1}{N}K^<(t-t')B^<(t,t'), \tag{3.9}$$

$$\Pi^<(t,t')=\frac{1}{N}\sum_m K^>(t'-t)G^<_m(t,t'). \tag{3.10}$$

The equivalent integral equations are

$$G^<_m(t,t')=\int dt_1 G^R_{\rm eq}(t-t_1)\int dt_2\{[\delta\epsilon_m(t_1)\delta(t_1-t_2) +\Sigma^R(t_1,t_2)-\Sigma^R_{\rm eq}(t_1-t_2)]G^<_m(t_2,t') +\Sigma^<(t_1,t_2)G^A_m(t_2,t')\} \tag{3.11}$$

and

$$B^<(t,t')=\int dt_1 B^R_{\rm eq}(t-t_1)\int dt_2 \times\{[\Pi^R(t_1,t_2)-\Pi^R_{\rm eq}(t_1-t_2)]B^<(t_2,t') +\Pi^<(t_1,t_2)B^A(t_2,t')\}. \tag{3.12}$$

B. Single level

Both integrodifferential and integral equations for G^R and $G^<$ are the same as in the case of the degenerate level. The self-energies are much simpler:

$$\Sigma^R(t,t')=\Sigma^R_{\rm eq}(t-t')=K^R(t-t') \tag{3.13}$$

and

$$\Sigma^<(t,t')=\Sigma^<_{\rm eq}(t-t')=K^<(t-t'). \tag{3.14}$$

IV. LINEAR RESPONSE AND DYNAMIC SUSCEPTIBILITIES

With the full general time-dependent solutions at hand the derivation of the linear-response approximation is no problem. All the quantities in the following are written as sum of equilibrium quantity and the deviation from equilibrium caused by $\delta\epsilon_m(t)$ [see Eq. (2.2)]. For example,

$$G^R_m(t,t')=G^R_{\rm eq}(t-t')+\delta G^R_m(t,t'), \tag{4.1}$$

with similar definitions holding for the deviations from equilibrium of the other quantities. Then the equations of Sec. III are linearized, i.e., all terms containing the deviations in quadratic or higher order are neglected. The double Fourier transform of deviations such as $\delta G^R_n(t,t')$ vanishes unless its two frequencies ω and ω' are related by $\omega'=\omega+\Omega$. The frequency Ω is a parameter, rather than an active variable, in the linearized equations, so we can take the Fourier transforms to depend on a single active variable ω, defining, for example $\delta G^R_m(\omega)$ by

$$\delta G^R_m(t,t')=\exp(-i\Omega t)\int\frac{d\omega}{2\pi}\exp[-i\omega(t-t')]\delta G^R_m(\omega). \tag{4.2}$$

The same defining relation is applied for the other propagators and self-energies.

A. Charge response of degenerate level

For the charge response, $\alpha_m=1$ so that none of the quantities depend on m; therefore we omit this subscript in the equations in this subsection. By linearizing Eqs. (3.5), (3.6), (3.3), and (3.4), respectively, we obtain the following equations for the retarded functions:

$$\delta G^R(\omega)=G^R_{\rm eq}(\omega+\Omega)[\delta\epsilon+\delta\Sigma^R(\omega)]G^R_{\rm eq}(\omega), \tag{4.3}$$

$$\delta B^R(\omega)=B^R_{\rm eq}(\omega+\Omega)\,\delta\Pi^R(\omega)B^R_{\rm eq}(\omega), \tag{4.4}$$

$$\delta\Sigma^R(\omega)=\int\frac{d\omega_1}{2\pi}\frac{1}{N}K^>(\omega-\omega_1)\,\delta B^R(\omega_1), \tag{4.5}$$

$$\delta\Pi^R(\omega)=\int\frac{d\omega_1}{2\pi}K^<(\omega_1-\omega)\,\delta G^R(\omega_1). \tag{4.6}$$

Similarly, by respectively linearizing Eqs. (3.11), (3.12), (3.9), and (3.10), we obtain the following equations for the lesser functions:

$$\delta G^<(\omega)=G^R_{\rm eq}(\omega+\Omega)(\delta\epsilon+\delta\Sigma^R(\omega))G^<_{\rm eq}(\omega) +G^<_{\rm eq}(\omega+\Omega)(\delta\epsilon+\delta\Sigma^A(\omega))G^A_{\rm eq}(\omega) +G^R_{\rm eq}(\omega+\Omega)\,\delta\Sigma^<(\omega)G^A_{\rm eq}(\omega), \tag{4.7}$$

$$\delta B^<(\omega)=B^R_{\rm eq}(\omega+\Omega)\,\delta\Pi^R(\omega)B^<_{\rm eq}(\omega) +B^<_{\rm eq}(\omega+\Omega)\,\delta\Pi^A(\omega)B^A_{\rm eq}(\omega) +B^R_{\rm eq}(\omega+\Omega)\,\delta\Pi^<(\omega)B^A_{\rm eq}(\omega), \tag{4.8}$$

$$\delta\Sigma^<(\omega)=\int\frac{d\omega_1}{2\pi}\frac{1}{N}K^<(\omega-\omega_1)\,\delta B^<(\omega_1), \tag{4.9}$$

$$\delta\Pi^<(\omega)=\int\frac{d\omega_1}{2\pi}K^>(\omega_1-\omega)\,\delta G^<(\omega_1). \tag{4.10}$$

Once the above four equations are solved, it is a straightforward matter to calculate $\chi_{\rm charge}(\Omega)$ using

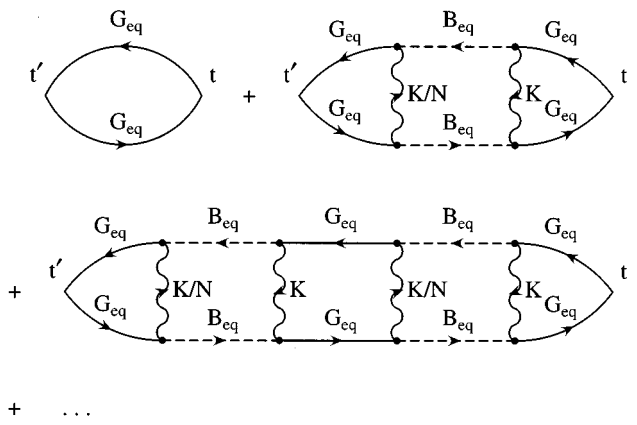

FIG. 3. Diagrammatic representation of the dynamic charge susceptibility in the NCA: $\chi_{\text{charge}}(t-t')=-N$ times the retarded part of the displayed sum of diagrams. The magnetic response is determined by the first diagram only.

$$\delta\langle n_m\rangle(\Omega)=\int\frac{d\omega}{2\pi}\,\delta G^{<}(\omega). \tag{4.11}$$

Then according to Eqs. (2.4) and (2.6) with $\alpha_n=1$, the charge susceptibility is

$$\chi_{\text{charge}}(\Omega)=-N\int\frac{d\omega}{2\pi}\,\frac{\delta G^{<}(\omega)}{\delta\epsilon}. \tag{4.12}$$

The charge susceptibility can be represented graphically by the diagrams, in Fig. 3. For deriving the equations given above from the diagrams, one must take care of the proper projection on the subspace $Q=1$. Q conservation can also be used to derive the alternative formula for χ_{charge},

$$\chi_{\text{charge}}(\Omega)=\int\frac{d\omega}{2\pi}\,\frac{\delta B^{<}(\omega)}{\delta\epsilon}, \tag{4.13}$$

as discussed in Appendix B.

A thermodynamical self-consistent scheme via a generating functional for calculating general susceptibilities in the NCA was suggested by Kuramoto.[37] It was applied for the calculation of the magnetic susceptibility; if it were to be applied for the charge susceptibility it should coincide with the results in the present paper. Finally a direct derivation with the Kubo formula via the *n*-*n* correlation function is also possible (compare Ref. 66). Then one must take care to select the appropriate diagrams (Ref. 37, Appendix G in Ref. 62). Jin and co-workers,[66] whose work we discuss further in Appendix B, apply different schemes for different parameter regimes.

B. Numerical procedure

After solving for the equilibrium functions by standard procedures, the linear-response equations are solved by iteration. The set of iterations for the retarded functions is started with

$$\delta G^{R}(\omega)=\delta\epsilon G^{R}_{\text{eq}}(\omega+\Omega)G^{R}_{\text{eq}}(\omega), \tag{4.14}$$

then we calculate $\delta\Pi^{R}(\omega)$, $\delta B^{R}(\omega)$, $\delta\Sigma^{R}(\omega)$, $\delta G^{R}(\omega)$, and so on. The set of iterations for the lesser functions is started with

$$\delta G^{<}(\omega)=G^{R}_{\text{eq}}(\omega+\Omega)(\delta\epsilon+\delta\Sigma^{R}(\omega))G^{<}_{\text{eq}}(\omega)+G^{<}_{\text{eq}}(\omega+\Omega)\times(\delta\epsilon+\delta\Sigma^{A}(\omega))G^{A}_{\text{eq}}(\omega), \tag{4.15}$$

and then we proceed in analogy. Typically 10–20 iterations were required for convergence, although at low Ω and N an order of magnitude more were sometimes required. In terms of the number of grid points, the convergence was monotonic and slow, the error appearing to diminish only a bit faster than $\sim C/n_p$, where n_p is the number of points within the lowest-energy scale of the problem (T_K in the most difficult cases). Typically n_p's of 10^2–10^3 were required for stable results. The constant C appeared to be substantially smaller in magnitude (opposite in sign) for χ_{charge} calculated from Eq. (4.13) than for χ_{charge} calculated from Eq. (4.12), leading to rather faster convergence for the former, a fact that was exploited at low frequency and temperature, where $|C|$ tends to be large.

C. Magnetic response of degenerate level

For the magnetic response everything works correspondingly. For example, from Eq. (3.4) one finds that

$$\delta\Pi^{R}(\omega)=\frac{1}{N}\sum_m\int\frac{d\omega_1}{2\pi}K^{<}(\omega_1-\omega)\,\delta G^{R}_m(\omega_1), \tag{4.16}$$

instead of Eq. (4.6). Similarly, the equation analogous to Eq. (4.3) is

$$\delta G^{R}_m(\omega)=G^{R}_{\text{eq}}(\omega+\Omega)[\alpha_m\delta\epsilon+\delta\Sigma^{R}(\omega)]G^{R}_{\text{eq}}(\omega), \tag{4.17}$$

while Eqs. (4.4) and (4.5) remain unchanged. Inserting Eq. (4.17) into Eq. (4.16) and using $\Sigma_m\alpha_m=0$ gives

$$\delta\Pi^{R}(\omega)=\int\frac{d\omega_1}{2\pi}K^{<}(\omega_1-\omega)G^{R}_{\text{eq}}(\omega+\Omega)\,\delta\Sigma^{R}(\omega)G^{R}_{\text{eq}}(\omega). \tag{4.18}$$

Equations (4.18), (4.4), and (4.5) form a closed set of equations for $\delta\Pi^{R}$, δB^{R}, and $\delta\Sigma^{R}$, but since there is no driving term, they imply that these quantities all vanish. For the retarded part there is only one equation of interest, which is Eq. (4.17) with $\delta\Sigma^{R}=0$. Using the same argument for the lesser quantities, one finds similarly that only $\delta G^{<}_m$ is different from zero:

$$\delta G^{<}_m(\omega)=\alpha_m\delta\epsilon[G^{R}_{\text{eq}}(\omega+\Omega)G^{<}_{\text{eq}}(\omega)+G^{<}_{\text{eq}}(\omega+\Omega)G^{A}_{\text{eq}}(\omega)]. \tag{4.19}$$

Then, since

$$\sum_m\,\delta\langle n_m\rangle(\Omega)=\sum_m\int\frac{d\omega}{2\pi}\alpha_m\delta G^{<}_m(\omega), \tag{4.20}$$

one finds, upon substitution of Eq. (4.19) and use of Eqs. (2.5) and (2.6), that

$$\chi_{\rm magn}(\Omega) = -N \int \frac{d\omega}{2\pi} [G^R_{\rm eq}(\omega+\Omega) G^<_{\rm eq}(\omega) + G^<_{\rm eq}(\omega+\Omega) G^A_{\rm eq}(\omega)]. \quad (4.21)$$

Since the magnetic susceptibility can be directly calculated from equilibrium quantities, there is no necessity for an iterative process (i.e., for a summation of diagrams), as for the charge susceptibility.

The graphical representation for the magnetic response is given by the first term in Fig. 3. Closed fermion loops do not contribute to the magnetic response ($\Sigma_m \alpha_m K \ldots G \ldots G \ldots = 0$) so all the other terms in Fig. 3 are zero. Formula (4.21) for the magnetic susceptibility has been given before [Eq. (4.2) in Ref. 56, Eq. (10) in Ref. 57, and Eq. (5.70a) in Ref. 62]. The derivation here generalizes these to less specific spatial symmetries.

D. Response of single level

The equations for the response have the following forms:

$$\delta G^R(\omega) = \delta\epsilon G^R_{\rm eq}(\omega+\Omega) G^R_{\rm eq}(\omega), \quad (4.22)$$

$$\delta G^<(\omega) = \delta\epsilon [G^R_{\rm eq}(\omega+\Omega) G^<_{\rm eq}(\omega) + G^<_{\rm eq}(\omega+\Omega) G^A_{\rm eq}(\omega)], \quad (4.23)$$

and

$$\chi(\Omega) = -\int \frac{d\omega}{2\pi} \frac{\delta G^<(\omega)}{\delta\epsilon}. \quad (4.24)$$

The diagrammatic representation is once again the first term in Fig. 3.

V. RESULTS AND DISCUSSION

We begin this section with some preliminary discussion of energy scales and spectral densities, and present what we found to be a remarkably successful approximation to $\chi_{\rm charge}$, which we call the spectral density convolution approximation (SDCA). Then in Sec. V B below we present results for $N=20$ as one approaches the Kondo regime, and in Sec. V C compare them with mean-field theory results. In Sec. V D we present results for the more nearly practical case $N=6$ in all three regimes: empty orbital, mixed valence, and Kondo.

A. Spectral densities and the spectral density convolution approximation

In order to facilitate the discussion, we present Fig. 4, which shows the real spectral functions for thermal equilibrium, for a level position $\epsilon=-1.5$ approaching the Kondo regime for the large N case. Here the Haldane invariant level position [Eq. (C1)] $\epsilon^*=-0.78$. We show both the total and occupied spectral functions times N. For the latter, the area under the curve is just the occupancy of the atomic orbital $\langle n\rangle$, in this case 0.92. For the former, the area would be just the orbital degeneracy N (here $N=20$) if it were not for the fact that the infinite U has pushed a substantial part of the spectral weight off to infinity, leaving behind at finite frequency, an area of 2.48 in this case, in agreement with Eq. (A17). For comparison we also show the equivalent functions for a single level ($N=1$, $U=0$) with the same parameters. Here the total spectral weight is 1 and the occupied part gives $\langle n\rangle = 0.86$.

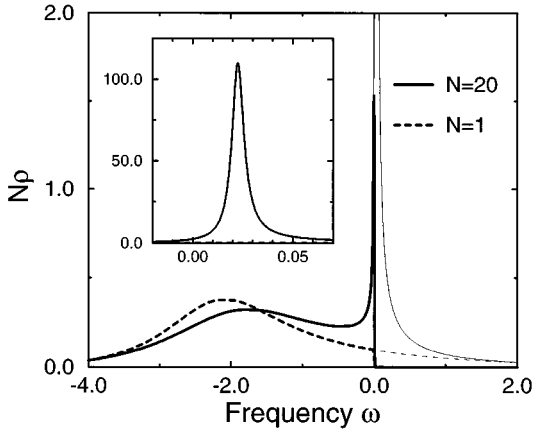

FIG. 4. N times the real spectral density ρ for $\epsilon=-1.5$ and $T=0.002$, with ρ according to Eq. (A15) for $N=20$ and Eq. (A19) for $N=1$. The occupied portions [Eqs. (A16) and (A20)] are indicated with heavier lines. The inset details the Kondo resonance which peaks above the Fermi level at $T_0\approx 0.022$. The total charge $\langle n\rangle$ is 0.92 for $N=20$ and 0.86 for $N=1$.

The Kondo resonance is centered at an energy T_0 above the Fermi level. Here we find $T_0\approx 0.022$, in good order-of-magnitude agreement with the Kondo temperature $T_K=0.018$ as calculated from the Bethe ansatz formula[63,62]

$$T_K = \frac{D_r}{2\pi} e^{1+C-3/2N} \left(\frac{\Delta}{\pi D_r}\right)^{1/N} e^{-\pi|\epsilon|/\Delta}. \quad (5.1)$$

The derivation of Eq. (5.1) essentially assumed a rectangular band, that is $-{\rm Im}K^R(\omega)=\Delta$ for $|\omega|\le D_r$ rather than Eq. (2.13), but we used a logarithmic scaling argument[43] to obtain $D_r\approx e^{-1/2}D$ so that $D_r\approx 3$ in our case where $D=5$. In principle one should also distinguish a temperature scale T_L which differs from T_K by a factor of the N-dependent Wilson number (≈ 1), but that distinction is beyond the accuracy scale of the discussion here, and we will always talk of T_0, T_K, and T_L as if they were the same.

The temperature in Fig. 4 is chosen about ten times lower than T_0 ($T=0.002$), therefore the width and position of the Kondo peak are close to their values at $T=0$; that is, there should be no significant changes as the temperature is further lowered. Of course, within the NCA there are changes as the temperature is lowered, where a spurious peak appears at the Fermi level. The temperature $T^*_{\rm NCA}$ at which this NCA breakdown occurs, as given by Eq. (5.53) of Ref. 62, is $T^*_{\rm NCA}=0.001$, although our actual calculations suggest that the breakdown does not occur until the temperature gets somewhat lower than this.

With increasing temperature there is almost no change in the charge for the single-level case, whereas for the degenerate level one can observe a change from a low-temperature value (0.92) to a value at higher temperature (0.98) (strong coupling to weak coupling, see, e.g., Schlottmann,[71] Fig. 5.1 a). When T becomes larger than T_0, the Kondo resonance becomes broader, and gradually vanishes.

We conclude this section with a discussion of a simple approximation for χ_{charge} which we call the spectral density convolution approximation (SDCA), which rather remarkably we have found to be accurate over a wide range of the parameter space. To motivate it, suppose we had an uncorrelated (one-body) N component Fermi system with density of states $\rho(\omega)$. Then the dissipative part of χ_{charge} for such a system would be given by

$$2\,\text{Im}\chi_{\text{charge}} = 2\pi N \int d\omega\, \rho(\omega)\rho(\omega+\Omega)[f(\omega)(1-f(\omega+\Omega)) - f(\omega+\Omega)(1-f(\omega))]. \tag{5.2}$$

The first term could be thought of as representing absorption of a vibrational quantum by electronic transitions from occupied states to unoccupied ones, while the second term as giving the contribution of the corresponding emission processes. Thus the SDCA consists of simply noting that for our system $\rho(\omega)$ is given by Eq. (A15), and then using this in Eq. (5.2) for χ_{charge}, despite the fact that our system is obviously not uncorrelated. We have found empirically by comparison with the calculations, which are exact within NCA, that the SDCA is valid in the empty orbital and mixed valence regimes, and also in the Kondo regime if $T > T_0$; and if Ω is large (>0.5) it is valid at all temperatures in the Kondo regime.

That the SDCA should work so well is rather remarkable, because it indicates that all vertex corrections are negligible when χ is calculated in this manner. This is not the same as the NCA procedure of neglecting the crossed vertex corrections in calculating the real spectral functions from G and B [see Eqs. (A13) and (A14)], but one must also neglect the type of vertex corrections one generates from the iteration of Eqs. (4.3) and (4.7), or from terms beyond the first term in Fig. 3. The latter, however, are virtually never negligible, even qualitatively. This means that corrections like these, which would also occur in the four-line correlation function to which Eqs. (5.2) and (A15) are zeroth approximations, must be mostly canceled by further vertex corrections in this correlation function. Yet, this probably cannot be explained by some undiscovered Ward identity, because the SDCA is not exact within NCA, and is not even approximate as T goes much below T_0 unless Ω is large.

Here we use the SDCA principally as an aid in the physical interpretation of our results, although in discussing friction it is used as an interpolation-extrapolation tool. Except there, however, the real spectral functions are not used in any of the calculations. This is an important point, because the most significant error made in the NCA occurs[40] in obtaining the real spectral functions from the ''auxiliary'' quantities G and B. Here all our principal results below follow directly from the auxiliary quantities alone.

B. NCA susceptibilities at large N

Here we present our results for the NCA susceptibilities at $N=20$. In Sec. V C we will compare them to results calculated using the mean-field theory of Coleman. The dynamic charge susceptibility is shown in Fig. 5. At high temperature, the Kondo feature in the spectral density is wiped out, leaving only one relevant energy scale. The response has a peak

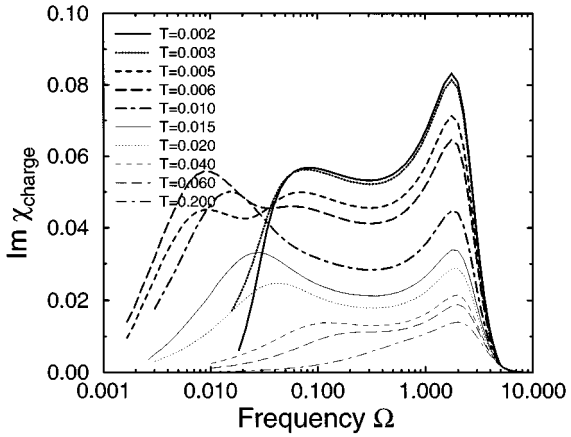

FIG. 5. Dynamic charge susceptibility in the NCA for $N=20$ and $\epsilon=-1.5$ at different temperatures T.

at about $\Omega=2$. As we will see below, this energy is close to the response peak for the single level. With lower temperature the Kondo feature in the spectrum (see Sec. V A) becomes more pronounced, and we observe a second peak in the response at about $\Omega=0.02$ (about T_0). The interpretation of the charge response for high frequencies and for $T \gtrsim T_0$ using the SDCA is quite easy: the peak in the response at about $\Omega=2$ is essentially due to transitions from the occupied states around the shifted level (centered at $\omega\sim-2$ in the spectral weight) to empty states close to and above the Fermi level. The peak at about $\Omega=0.02$ is due to transitions from occupied states close to, but below, the Fermi level into the unoccupied states in the Kondo resonance. This interpretation is of course oversimplified, as it does not take into account the strong temperature dependence of the Kondo resonance itself, which causes the low-frequency response peak to shift quite a bit with temperature.

The SDCA becomes wrong for lower frequencies (here below, say, $\Omega=0.5$) and temperatures below T_0. First the low-frequency peak shifts to lower frequencies (e.g., $\Omega=0.01$ for $T=0.01$). With lower temperatures (strong-coupling limit) we observe a two-peak structure with the left peak now much closer to the right peak; we will show below that this form of the curve agrees very well with the mean-field results around $T=0$. Though the NCA cannot be applied for temperatures too low we believe for the parameters chosen our calculation at $T=0.002$ to be close to a temperature where the dynamic charge response saturates. The proximity of the $T=0.002$ and 0.003 curves can be seen as a sign of this saturation. These were the lowest temperatures feasible for low frequency with the present numerical method. At the lowest temperatures the low-frequency charge response is cut off below roughly $\Omega\approx0.07$, just in the region where the magnetic response starts to peak (see below). This feature is preserved in mean-field theory (see Sec. V C).

In Fig. 6 we show the imaginary part of the dynamic magnetic susceptibility for the degenerate level. Calculations like that have been done before.[56,72] They are included here in order to facilitate the discussion and to make a comparison with mean-field theory. There is a broad peak for higher temperatures which shifts at lower temperatures. For $T<0.005$ (as in the charge response) the magnetic response locks into the low-temperature (strong coupling) behavior.

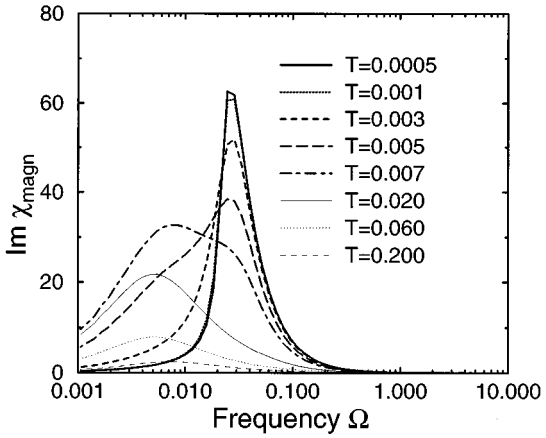

FIG. 6. Dynamic magnetic susceptibility in the NCA for $N=20$ and $\epsilon=-1.5$ at different temperatures T.

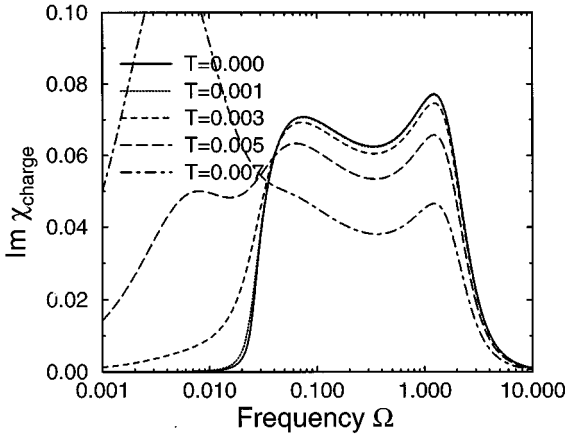

FIG. 7. Mean-field approximation of the dynamic charge susceptibility for the degenerate level ($N=20$) according to Coleman's formula (C3) for $\epsilon=-1.5$ or $\epsilon^*=-0.782$. [Parameters from (C2): At $T=0$, $\tilde{\epsilon}=0.025$ and $\tilde{\Delta}=0.0037$; at $T=0.007$, $\tilde{\epsilon}=0.028$, and $\tilde{\Delta}=0.0022$].

Here there is one narrow peak which is located at $\Omega\approx 0.025$. This is roughly the position of the Kondo resonance T_0. The response is completely determined by the auxiliary G function, which has only one energy scale set by T_K, which in turn determines the magnetic response. The level position ϵ does not play a role (except indirectly through the determination of T_K). Once again we can choose T low enough to see the response saturate. Although $T=0.0005$ is slightly below T^*_{NCA} [see Eq. (5.53) of Ref. 62], it is still too high to observe the spurious NCA singularities for low frequency.[72] When plotting $\mathrm{Im}\chi(\Omega)/\Omega$ one can observe Lorentzian behavior for higher temperatures and a resonance feature at $\Omega\approx 0.025$ at lower temperatures, that was similarly seen before.[72] The absolute values are very large, much larger than the charge response, as expected from simple arguments.

C. Comparison with mean-field theory

Here we compare the $N=20$ results in the Kondo regime with the mean-field theory of Coleman [see Appendix C for details]. He studied the infinite-U Anderson model by considering fluctuations around a broken-symmetry mean-field theory in leading order in $1/N$.[64] He calculated numerical results for the dynamic susceptibilities for $T=0$, and his formulas can be applied for finite though small temperatures, too. His results are valid in a limit where NCA calculations become wrong. We will try to make a connection between our finite-temperature NCA results and Coleman's low-temperature results. The mean field theory results have been shown[65] to be exact for $N=\infty$ for any finite filling factor Q/N. Here we apply them for $N=20$ and $Q/N=\frac{1}{20}$ where it could be hoped that they still would be a good approximation, although they obviously break down as T approaches the temperature of the mean-field phase transition, which does not occur for any finite N. The NCA should also be very accurate for an N this size, but it breaks down for T's less than T^*_{NCA}. Since T^*_{NCA} is typically less than where the mean-field phase transition occurs, it might be hoped that there would be a region of overlap.

There are several difficulties when directly comparing Coleman's results and our NCA results. Coleman uses a Lorentzian density of band states $(-\mathrm{Im}K^R(\omega)=\Delta[1+(\omega/D_L)^2]^{-1})$ whereas our density is parabolic [see Eq. (2.13)]. The difference is roughly compensated for by setting $D_L=D\ \exp(-1/2)$. While Coleman's results are valid for a wide band, our numerical NCA calculation is applied for cases with bands that cannot be called very wide (e.g., $D=5\Delta$ and $D_L\approx 3\Delta$). Furthermore it is not clear how far in the Kondo limit one has to be ($|\xi|\ll\Delta$) for Coleman's formulas to be applicable. Next, the population of the atomic level will not perfectly coincide. Also, while the mean-field results are valid for $T=0$ and for very small temperatures, and the NCA results for temperatures that are not too low, it is not clear whether there should be some overlap of the two approaches for temperatures in between, or, if there is a temperature ''gap,'' what the susceptibilities might look like there. With all these restraints in mind, it will turn out that both approaches can be very reasonably connected and we can gain a very good insight into the behavior of the susceptibilities over the whole temperature range.

In Figs. 7 and 8 we show the imaginary part for the charge and magnetic dynamic response calculated with Cole-

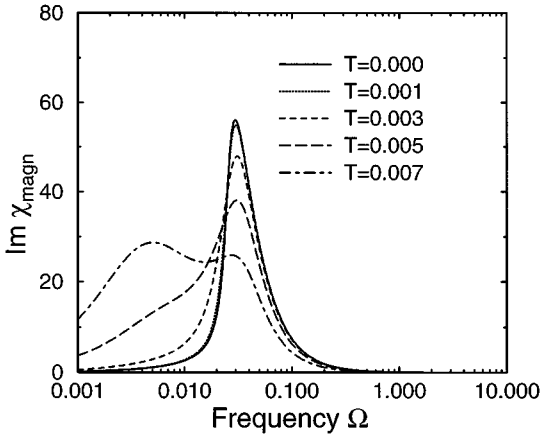

FIG. 8. Mean-field approximation of the dynamic magnetic susceptibility for the degenerate level ($N=20$) according to Coleman's formula (C4) for $\epsilon=-1.5$ or $\epsilon^*=-0.782$.

man's formulas (C3) and (C4). The figures should be compared with Figs. 5 and 6. We find an agreement that is by far better than qualitative. Taking into account the different sort of approach and all the problems for a direct comparison that were discussed above, there is a surprisingly good agreement for temperatures between roughly 0.001 to 0.005, concerning both absolute values and characteristic frequencies. The mean-field phase transition for $N=\infty$ occurs for $T\sim 0.01$, and the mean-field results for finite N should be expected to grow poor as T nears this value. Our NCA results show how the low-frequency peak in the charge susceptibility, which increases in strength in mean-field theory as the temperature is raised, turns around and begins to decrease again, and ultimately disappears at high temperatures. Coleman himself applied his formulas only for $T=0$. Our comparison shows that they can be applied for small finite T, too. It also suggests that NCA and mean-field theory have a regime of common validity, thus bridging the gap between low and high temperatures.

D. NCA susceptibilities in various regimes for $N=6$

Here we present and discuss results for the empty orbital, mixed-valent, and Kondo regimes. We will try to relate our discussion where possible to concepts that might be important for electronic damping of atomic motions or friction at metal surfaces. For the latter purpose one should think of a resonance half-width Δ on the order of an eV, and temperatures and frequencies varying through a range that is typically around 0.01–0.1 times this. To simplify the numerics we chose to present the results for $N=6$, although $N=2$ or possibly $N=4$ are more typical for real surface problems to which the model would most cleanly apply. Here we will simply be content to say that we have made preliminary calculations for $N=2$, and found that they are qualitatively similar to the $N=6$ ones.

When presenting the results, we always give for comparison the single-level ($N=1$, $U=0$) results, in order to emphasize the vast qualitative differences that can occur. To make this comparison we choose the Δ parameter for $N=6$ to be the same as for $N=1$ (and as before use this parameter as the unit for all other quantities). This has the effect that the (large) width of an atomic state below the Fermi level is roughly the same for $N=1$ as it is for $N=6$ (i.e., Δ). On the other hand, when the level is above the Fermi level in the empty orbital regime, the level width is roughly Δ/N, so that the width in the single-level model will be larger by a factor of N than in the correlated model. Recall that our Δ is the quantity that has been called $N\Delta$ in a number of previous papers.

We begin with the empty orbital regime, where we show the results in Fig. 9. Here, in the context of the SDCA, the contributions come from transitions from the tail of the density of states below the Fermi level to the broadened atomic level above. One does not expect the correlation effects to play a significant role for the empty level, and the curves show this at least qualitatively, with little anomalous temperature dependence except at extreme temperatures. Nevertheless for obtaining results that are correct within factors of 2, the correlation effects are still important, as shown by the fact that the magnetic and charge susceptibilities are still a little different. The fairly substantial difference in sharpness (especially at low frequencies) between $N=1$ and 6 is to a good degree due the point discussed above, that the width of the level is Δ/N and not Δ, so that we are comparing transitions in states with different widths.

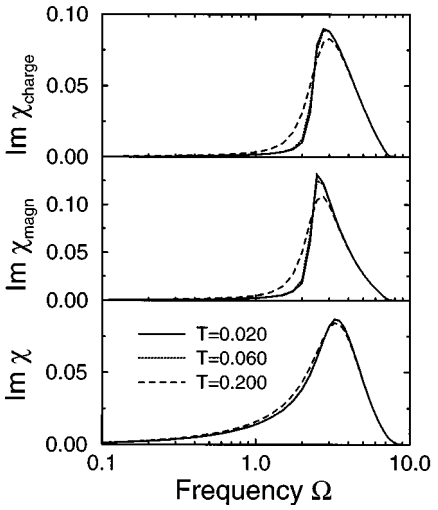

FIG. 9. Dynamic susceptibilities in the empty impurity regime ($\epsilon=2$). The top and middle panels are for $N=6$ [$\langle n\rangle=0.08$], while the bottom panel is for $N=1$ [$\langle n\rangle=0.10$].

We now consider Im $\chi_{\rm charge}(\Omega)/\Omega$, which at low frequencies is related to the electronic friction as discussed in Sec. II E. If this quantity is constant in the range of frequencies appropriate to the atomic motion, then the system will behave as it had a friction constant $K=M\gamma(\Omega)$, where γ is given by Eq. (2.18). From the curve for $N=1$ in Fig. 9 we find that $\mathrm{Im}\chi_{\rm charge}(\Omega)/\Omega=0.013$, in good agreement with the exact low-frequency value for the wide-band model

$$\mathrm{Im}\chi_{\rm charge}(\Omega)/\Omega=\frac{1}{\pi}\frac{\Delta^2}{(\epsilon^2+\Delta^2)^2}=0.0127. \qquad (5.3)$$

Except for the highest temperature, one finds for $N=6$ that $\mathrm{Im}\chi_{\rm charge}(\Omega)/\Omega\sim 0.0015$ in the lower half of the frequency range shown in the figure. A good part of the difference between this and the friction for the single-level model ($U=0$) is due to the difference in level widths discussed above. In the empty orbital regime, the most comparable $U=0$ case would be obtained by letting $\Delta\to\Delta/N$ in Eq. (5.3) and then multiplying the results by N, thus replacing Eq. (5.3) by

$$\mathrm{Im}\chi_{\rm charge}(\Omega)/\Omega=\frac{1}{\pi N}\frac{\Delta^2}{(\epsilon^2+(\Delta/N)^2)^2}=0.0033, \quad (5.4)$$

which is only on the order of a factor of 2 different from the value for $\chi_{\rm charge}$ in Fig. 9. It turns out that Eq. (5.4) is exact in the correlated case only to lowest order in Δ/ϵ. The correction term is much larger than that implied by the Δ^2/N^2 term in the denominator of Eq. (5.4); it in fact makes a fractional reduction to Eq. (5.4) of order Δ/ϵ times logarithmic terms, as may be straightforwardly verified by perturbation theory in V_k. Thus the difference between our result (~ 0.0015) and Eq. (5.4) is not inconsistent with what should be expected. We conclude that even in this empty orbital

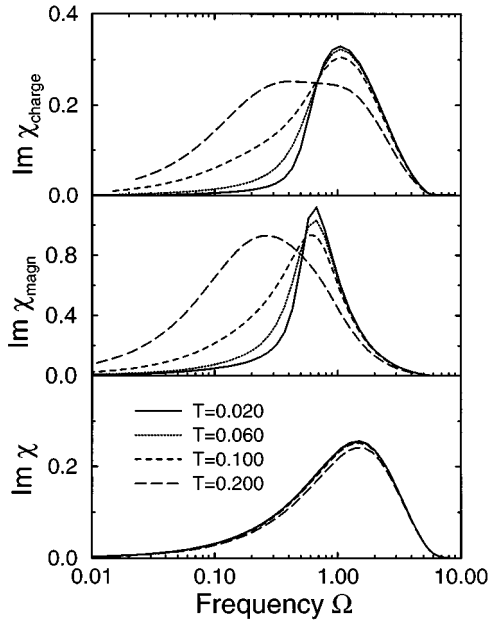

FIG. 10. Dynamic susceptibilities in the mixed-valence regime ($\epsilon=0$). The top and middle panels are for $N=6$ [$\langle n\rangle=0.4$], while the bottom panel is for $N=1$ [$\langle n\rangle=0.5$].

regime where the strong-U correlations effects do not produce much temperature dependence, they are still important if quantitative results are required. The friction is very small here, because the atomic level is well above the Fermi level.

The susceptibilities in the mixed-valent region are shown in Fig. 10. They are of course much larger in this region. The influence of the large-U correlation effects are evident not only from the temperature dependence, but the difference between the magnetic and charge susceptibilities.

A nonlogarithmic plot of $\chi_{\rm charge}$ at the low-frequency end of the figure shows that the curves apparently approach straight lines through the origin, suggesting that a sensible frictionlike regime [see Eq. (2.18)ff.] has been reached, albeit with strongly temperature-dependent friction. This can be understood given that the SDCA is a good approximation in this region: for $\Omega\ll T$, Eq. (5.2) becomes

$$\frac{{\rm Im}\chi_{\rm charge}(\Omega)}{\Omega}=\pi N\int d\omega\,\rho^2(\omega)\left(-\frac{df(\omega)}{d\omega}\right). \qquad (5.5)$$

The form of $\rho(\omega)$ for this case is a single peak whose maximum is about 0.5Δ above the Fermi level, and whose width is $\sim 0.2\Delta$, but temperature dependent, increasing by $\sim 50\%$ as the temperature is increased over the range of the curves in the figure. Thus Eq. (5.5) suggests that the friction is determined by the overlap of the tail of $-df(\omega)/d\omega$ and the lower end of the peak in $\rho^2(\omega)$. As an illustration of this and of the interesting temperature dependences that can occur, we show a plot of the prediction of Eq. (5.5) in Fig. 11. We note that this is consistent with the results from the full NCA calculations for the case $\epsilon=0$. The SDCA curves show in greater detail the transition to the Kondo regime as the temperature is lowered.

One should note that, unlike the uncorrelated $U=0$, $N=1$ case, the value $\epsilon=0$ is not special. In the former case $\rho(\omega)$ just consists of a Lorentzian-like curve that follows ϵ around, including crossing the Fermi level when ϵ does. In the correlated case, the peak does not cross the Fermi level as ϵ is lowered, but rather remains as if suspended above the Fermi level, sharpening, and weakening as it turns into the Kondo resonance, with the broad peak at the atomic level position reappearing below the Fermi level as ϵ is further lowered. The configuration leading to the strongly temperature-dependent friction persists for a range of ϵ in the mixed-valent regime, and is not unique to our choice $\epsilon=0$. All this is clear from the curves in Fig. 11. As ϵ moves further below the Fermi level, the resonance in the spectral density, which is still above the Fermi level, sharpens into the Kondo resonance, and the characteristic low-energy scale comes within the range of temperatures shown in Fig. 11. For temperatures exceeding this range, the Kondo peak in the spectral density weakens, and so does the friction as the temperature increases further.[73] This high-temperature falloff of Imχ with increasing T is seen again in the figures, where we display the charge susceptibility in the Kondo regime. An explicit plot of the rapid temperature dependence of the dissipation in the Kondo regime is given in Ref. 48.

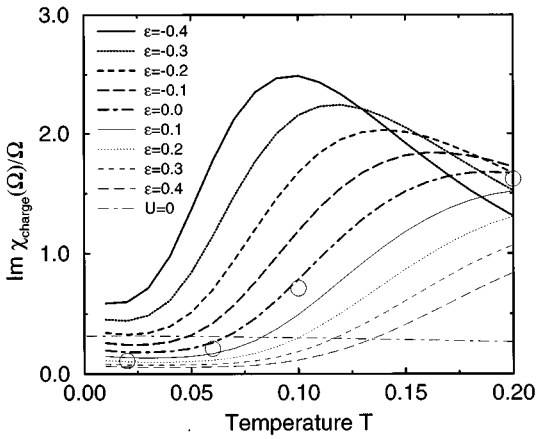

FIG. 11. Friction in the mixed-valence regime in the SDCA via Eq. (5.5), for various values of orbital energy ϵ. The circles represent the full NCA for $\epsilon=0$, and were obtained by the slopes of the curves like those in Fig. 10 [vs Ω instead of $\log_{10}\Omega$] at $\Omega=0.03$. The curve marked $U=0$ is the single-level curve for $\epsilon=0$; values for other ϵ's are smaller and have weaker temperature dependence.

In contrast to this is the $U=0$ case, where the choice $\epsilon=0$ puts a peak in $\rho(\omega)$ right at the Fermi level. Then Imχ actually decreases with increasing temperature, as shown in Fig. 10. This can be understood from Eq. (5.5): at $T=0$, $-df(\omega)/d\omega$ samples only the central maximum of $\rho^2(\omega)$, while as T rises it begins to sample the tails as well. This inverse temperature dependence should decrease as ϵ moves away from the Fermi level, and should reverse itself when ϵ is a distance $\sim\Delta$ above or below the Fermi level. In Fig. 11 we show this single level $U=0$ curve, just for the case $\epsilon=0$, where it is largest. It is somewhat problematic how to make the best comparison between the two cases in this intermediate regime. We have continued to follow the scheme of keeping our Δ constant as we go from the single level to the degenerate level, a procedure that is clearly sensible in the Kondo regime. However one could argue that a smaller Δ would be more appropriate for the single-level case in the mixed-valent regime, and that then the single-

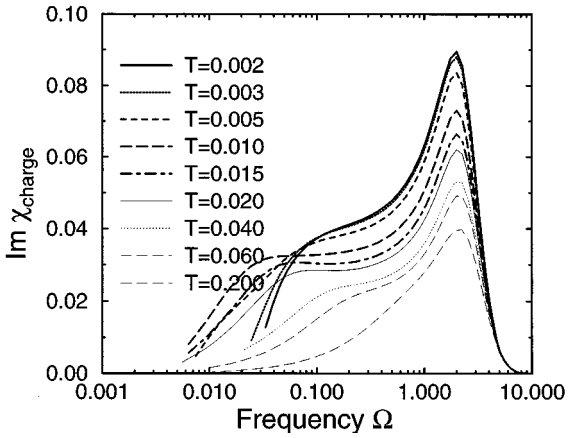

FIG. 12. Dynamic charge susceptibility for $N=6$ and $\epsilon=-1.5$.

level friction would be larger and more temperature dependent than what we have shown. It is in any case true without question, however, that the temperature dependence is *qualitatively* different in the two cases.

Finally, we show the results for $\epsilon=-1.5$, that is, approaching the Kondo regime, in Figs. 12, 13, and 14. As discussed previously for $N=20$, the results for the degenerate level case show strong temperature dependence on two different energy scales, as opposed to those for the single-level case which show essentially no temperature dependence except at the extreme temperature $T=0.2$. The charge susceptibilities are very small, as expected. However, the quantity relevant to electronic friction is $\mathrm{Im}\chi(\Omega)/\Omega$. This is as large as in the mixed-valent case, because of the very low-frequency response caused by the Kondo resonance. However, note also that we are not in the simple friction limit even at the lowest frequencies shown, and indeed $\mathrm{Im}\chi$ is neither a monotonic function of frequency nor of temperature. It can change by factors of 10 over a range of temperatures that are still just a small fraction of Δ. In short, we have an electronic energy scale which is as small as those normally associated with the vibrations of the nuclei, along with temperature dependences on this low scale, which can be of either sign.

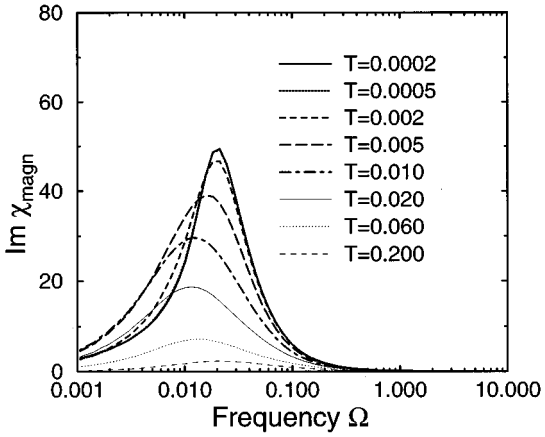

FIG. 13. Dynamic magnetic susceptibility for $N=6$ and $\epsilon=-1.5$.

VI. CONCLUSION

We have provided benchmark calculations of the predictions of the noncrossing approximation for the so-called charge susceptibility. These could be useful in several areas where the Anderson model is relevant, including highly correlated condensed-matter systems, quantum dots, and the motion of atoms and molecules outside metallic surfaces. With respect to the latter, we showed the connection between these results and electronic friction. We show that in two regimes, the effect of the intra-atomic Coulomb repulsion U can lead to temperature dependence of the electronic friction on a scale as small as that usually associated with vibrational processes. Both the temperature and frequency dependence are qualitatively different from models in which U is either neglected or treated in the Hartree-Fock approximation.

ACKNOWLEDGMENTS

We would like to thank Piers Coleman for discussions and for leaving his equilibrium program to us. One of us (T. B.) would like to thank Professor A. Hüller for his kind hospitality at Universität Erlangen-Nürnberg. This work was supported in part by the National Science Foundation under Grant Nos. DMR 91-34066 and DMR 94-07055, and by Deutsche Forschungsgemeinschaft.

APPENDIX A: EQUILIBRIUM SOLUTION

In equilibrium there is no variation of parameters $[\delta\epsilon(t)=0]$. Then we have the standard Anderson problem. Since the equilibrium quantities are needed for the linear-response solution, we show the most important formulas in a form appropriate for the real-time Green's-function terminology. When presenting the NCA equilibrium results, we refer especially to the work by Kuramoto[37] and Coleman.[39]

1. Degenerate level

With the Dyson equations in the usual form the self-energies in the NCA can be represented by the diagrams in Fig. 2, with the auxiliary propagators G and B replaced by their equilibrium counterparts. The various propagators and self-energies can be easily derived by applying the definitions.[67] The only thing one must especially take care of is the proper projection on the $Q=1$ subspace (for details, see Ref. 34). The retarded propagators are given by the following equations:

$$G^R_{\mathrm{eq}}(\omega)=[\omega-\epsilon-\Sigma^R_{\mathrm{eq}}(\omega)]^{-1}, \tag{A1}$$

$$B^R_{\mathrm{eq}}(\omega)=[\omega-\Pi^R_{\mathrm{eq}}(\omega)]^{-1}, \tag{A2}$$

$$\Sigma^R_{\mathrm{eq}}(\omega)=\int\frac{d\omega_1}{2\pi}\frac{1}{N}K^{>}(\omega-\omega_1)B^R_{\mathrm{eq}}(\omega_1), \tag{A3}$$

$$\Pi^R_{\mathrm{eq}}(\omega)=\int\frac{d\omega_1}{2\pi}K^{<}(\omega_1-\omega)G^R_{\mathrm{eq}}(\omega_1), \tag{A4}$$

and the lesser propagators by

$$G^<_{\mathrm{eq}}(\omega)=G^R_{\mathrm{eq}}(\omega)\Sigma^<_{\mathrm{eq}}(\omega)G^A_{\mathrm{eq}}(\omega), \tag{A5}$$

$$B^{<}_{\rm eq}(\omega)=B^{R}_{\rm eq}(\omega)\Pi^{<}_{\rm eq}(\omega)B^{A}_{\rm eq}(\omega), \tag{A6}$$

$$\Sigma^{<}_{\rm eq}(\omega)=\int\frac{d\omega_1}{2\pi}\frac{1}{N}K^{<}(\omega-\omega_1)B^{<}_{\rm eq}(\omega_1), \tag{A7}$$

$$\Pi^{<}_{\rm eq}(\omega)=\int\frac{d\omega_1}{2\pi}K^{>}(\omega_1-\omega)G^{<}_{\rm eq}(\omega_1). \tag{A8}$$

The retarded and lesser quantities are connected by thermal equilibrium relations like

$$G^{<}_{\rm eq}(\omega)=-2{\rm Im}G^{R}_{\rm eq}(\omega)\exp(-\beta\omega)/Z, \tag{A9}$$

with Z being the partition function for the adsorbate level, the latter being determined by the requirement that $Q=1$, as calculated from

$$Q=\int\frac{d\omega}{2\pi}[NG^{<}_{\rm eq}(\omega)+B^{<}_{\rm eq}(\omega)]. \tag{A10}$$

The spectral functions satisfy the sum rules

$$-\int\frac{d\omega}{\pi}{\rm Im}G^{R}_{\rm eq}(\omega)=-\int\frac{d\omega}{\pi}{\rm Im}B^{R}_{\rm eq}(\omega)=1. \tag{A11}$$

Due to Eq. (A10), the atomic level occupancy $\langle n\rangle$ can be calculated either from $G^{<}$ or $B^{<}$,

$$\langle n\rangle=N\int\frac{d\omega}{2\pi}G^{<}_{\rm eq}(\omega)=1-\int\frac{d\omega}{2\pi}B^{<}_{\rm eq}(\omega). \tag{A12}$$

The introduction of slave bosons makes both G and B auxiliary quantities. The physical adsorbate electron propagator A is given by the diagram in Fig. 1. Vertex corrections are not considered in the NCA. We have

$$A^{R}_{\rm eq}(\omega)=\int\frac{d\omega_1}{2\pi}[G^{R}_{\rm eq}(\omega+\omega_1)B^{<}_{\rm eq}(\omega_1)-G^{<}_{\rm eq}(\omega+\omega_1)B^{A}_{\rm eq}(\omega_1)] \tag{A13}$$

and

$$A^{<}_{\rm eq}(\omega)=-\int\frac{d\omega_1}{\pi}G^{<}_{\rm eq}(\omega+\omega_1){\rm Im}B^{R}_{\rm eq}(\omega_1). \tag{A14}$$

The real physical adsorbate electron spectral density $\rho(\omega)$ is given by

$$\rho(\omega)=-\frac{1}{\pi}{\rm Im}A^{R}_{\rm eq}(\omega). \tag{A15}$$

On the other hand $A^{<}_{\rm eq}(\omega)/2\pi$ is the physical adsorbate electron occupied spectral density. In this thermal equilibrium situation the two quantities are related by

$$\frac{A^{<}_{\rm eq}}{2\pi}(\omega)=\rho(\omega)f(\omega). \tag{A16}$$

Because we let $U\to\infty$ at the beginning, that part of the real spectral weight corresponding to multiple occupancy of the degenerate level is shifted to infinity and is not counted in the spectral sum rule, which in this case reads

$$-\int\frac{d\omega}{\pi}{\rm Im}A^{R}_{\rm eq}(\omega)=1-(1-1/N)\langle n\rangle. \tag{A17}$$

The quantity $(1-1/N)\langle n\rangle$ is simply the probability that one of the other $N-1$ degenerate levels is occupied when one tries to add an electron to the mth one. Nevertheless, one may still obtain the occupancy $\langle n\rangle$ from the $A^{<}$ spectrum,

$$\langle n\rangle=N\int\frac{d\omega}{2\pi}A^{<}_{\rm eq}(\omega). \tag{A18}$$

2. Single level

The self-energy in the single-level case is exactly given by $\Sigma^{R}_{\rm eq}(\omega)=K^{R}(\omega)$, and $\Sigma^{<}_{\rm eq}(\omega)=K^{<}(\omega)$. Here the real spectral density $\rho(\omega)$ is given by

$$\rho(\omega)=-\frac{1}{\pi}{\rm Im}G^{R}_{\rm eq}(\omega), \tag{A19}$$

while $G^{<}_{\rm eq}(\omega)/2\pi$ is the real occupied spectral density. Similarly to the degenerate case, the equilibrium quantities are related by

$$\frac{G^{<}_{\rm eq}(\omega)}{2\pi}=\rho(\omega)f(\omega). \tag{A20}$$

All the quantities can be given in closed form for the single-level case, and there is no approximation involved.

APPENDIX B: IDENTITIES AND RELATIONS

Here we list some of the identities and sum rules satisfied by the linear-response quantities, which we use or refer to in the main text, in addition to, of course, Kramers-Kronig,

$${\rm Re}\chi(\Omega)=P\int\frac{d\Omega'}{\pi}\frac{{\rm Im}\chi(\Omega')}{\Omega'-\Omega}, \tag{B1}$$

which along with its inverse follows for all response functions from causality. First the spectral density integrals (A11) remain unchanged; that is,

$$\int\frac{d\omega}{\pi}{\rm Im}\delta G^{R}_{m}(\omega)=\int\frac{d\omega}{\pi}{\rm Im}\delta B^{R}(\omega)=0. \tag{B2}$$

Second, $Q=1$ must still hold; that is,

$$\delta Q(t)\equiv\exp(-i\Omega t)\int\frac{d\omega}{2\pi}\left(\sum_{m}\delta G^{<}_{m}(\omega)+\delta B^{<}(\omega)\right)=0. \tag{B3}$$

This can be explicitly shown, most easily by showing $(d/dt)\delta Q(t)=0$ via the linearized integrodifferential equations. Therefore the charge susceptibility may be calculated either from Eq. (4.12) or (4.13), as stated in the text.

It is well known that for $T\to 0$ the NCA does not properly represent the Fermi-liquid regime.[58,57,62] Neglect of vertex

corrections destroys a proper description of low-energy excitations. Both the Friedel-Langreth relation[68] for the equilibrium spectral density

$$-\mathrm{Im}A^R_{\mathrm{eq}}(\omega=0)=\frac{N}{\Delta}\sin^2(\pi\langle n\rangle/N) \tag{B4}$$

and the Korringa-Shiba[74,75] relation

$$\lim_{\Omega\to 0}\frac{\mathrm{Im}\chi(\Omega)}{\Omega}=\frac{\pi}{N}(\chi(0))^2 \tag{B5}$$

for the magnetic response are known to be violated. The spectral density has a very small cusp around the Fermi energy $\omega=0$, and the magnetic susceptibility $\mathrm{Im}\chi(\Omega)/\Omega$ diverges for very low frequencies Ω. These singularities should show up for temperatures T lower than T^*_{NCA} which was specified by Bickers.[62] Presumably also the Korringa-Shiba relation for the charge response[71] is violated in a similar fashion in the NCA; numerically the limit on the left side of Eq. (B5) is hard to determine for χ_{charge}.

The violation of the Fermi-liquid relations can be seen as a consequence of the partial resummation of terms in all orders in $1/N$. Taking into account only diagrams that contribute in leading orders in $1/N$ can remedy this problem.[76,66] At frequencies around the Kondo temperature, however, there must be a summation of infinite orders to dispose of the Kondo divergence. Jin and co-workers[66] seem to follow this twofold strategy. It is very well suited for a general qualitative discussion and for deriving formulas for limiting cases (e.g., $T\gg T_K$, $T\ll T_K$, $\omega\approx T_K$, and $\omega\approx 0$). It is certainly less suited for quantitative numerical calculations (different formulas will not render continuous results). Jin, Matsuura, and Kuroda[66] are wrong in their 1991 paper when they claim to include ''crossing'' diagrams that are not contained in the NCA—they do not include crossing conduction electron lines, and all diagrams suggested in their paper are contained in our NCA calculation. What makes the difference from the NCA is the neglect of the self-consistency—the infinite summation of diagrams at low frequencies and temperatures and the calculation in leading order in $1/N$ instead.

It should be emphasized that besides the NCA there is an additional reason for the Korringa-Shiba relations not to be fulfilled, which is the neglect of impurity-band and band-band contributions in χ, which was defined just as the impurity-impurity correlation function. For a finite bandwidth these terms might not be negligible. So, for a finite band, even for the single-level model the Korringa-Shiba relation is not fulfilled. Only in the wide-band limit ($D\to\infty$ with $|V|^2/D$ finite) does the susceptibility for the single level satisfy the Korringa-Shiba relation, as usually stated.

APPENDIX C: LARGE-N MEAN-FIELD THEORY FOR DYNAMIC SUSCEPTIBILITIES IN THE KONDO LIMIT AT LOW TEMPERATURES

Here we present in our notation the formulas from Coleman's theory[64] relevant to the evaluation here. The bandwidth D_L and the level position ϵ enter only via the leading-order expression for the Haldane invariant level [see Eq. (2.32) of Ref. 64]

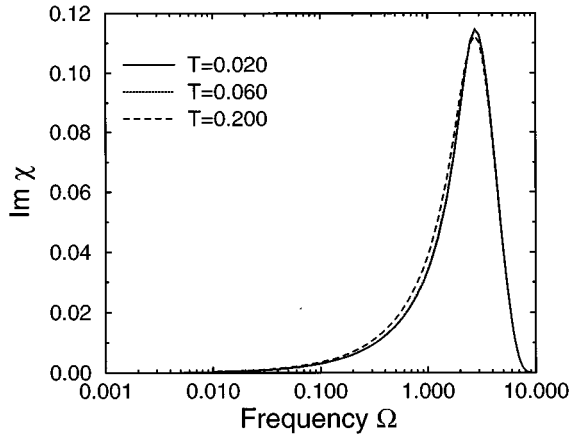

FIG. 14. Dynamic susceptibility for the single level for $\epsilon=-1.5$ at different temperatures.

$$\epsilon^*=\epsilon+\frac{\Delta}{\pi}\ln\frac{D_L\pi}{\Delta}. \tag{C1}$$

One has to determine the complex level position ξ with $\xi=\tilde{\epsilon}+i\tilde{\Delta}$ by solving the equation [see Eq. (2.29) of Ref. 64]

$$\frac{\Delta}{\pi}\left[\tilde{\psi}(\xi)-\ln\frac{\Delta\beta}{2\pi^2 i}\right]+\xi=\epsilon^*+\frac{i\Delta}{N}, \tag{C2}$$

with $\tilde{\psi}(\xi)=\psi(\frac{1}{2}+(\xi\beta/2\pi i))$, where ψ is the digamma function. The dynamic charge susceptibility is given by

$$\chi_{\mathrm{charge}}(\Omega)=\frac{N\tilde{\Delta}}{\Delta}\frac{\Omega}{\Omega+2i\tilde{\Delta}}\left\{\left[\frac{\Delta}{\pi}[\tilde{\psi}(\xi+\Omega)-\tilde{\psi}(\xi)]+\Omega\right]^{-1}+\left[\frac{\Delta}{\pi}[\tilde{\psi}(-\xi^*+\Omega)-\tilde{\psi}(-\xi^*)]-\Omega\right]^{-1}\right\}, \tag{C3}$$

and the dynamic magnetic susceptibility by [see Eq. (3.66) of Ref. 64]

$$\chi_{\mathrm{magn}}(\Omega)=-\frac{N\tilde{\Delta}}{\pi}\frac{1}{(\Omega+2i\tilde{\Delta})\Omega}\times[\tilde{\psi}(\xi+\Omega)-\tilde{\psi}(\xi)+\tilde{\psi}(-\xi^*+\Omega)-\tilde{\psi}(-\xi^*)]. \tag{C4}$$

The prefactors are chosen to be in accordance with our conventions above. Both susceptibilities fulfill the Korringa-Shiba relation in the form Eq. (B5). The limit $T\to 0$ can be easily performed [$\tilde{\psi}(\xi)\to\ln\xi\beta/2\pi i$].

[1] F. O. Goodman, Prog. Surf. Sci. **5**, 261 (1975).
[2] H. Schlichting, D. Menzel, T. Brunner, and W. Brenig, J. Chem. Phys. **97**, 4453 (1992).
[3] J. Los and J. J. C. Geerlings, Phys. Rep. **190**, 133 (1990).
[4] W. Heiland and A. Närmann, Nucl. Instrum. Methods Phys. Res. Sect. B **78**, 20 (1993).
[5] B. N. J. Persson and M. Persson, Solid State Commun. **36**, 175 (1980).
[6] R. Ryberg, Surf. Sci. **114**, 627 (1982).
[7] Ž. Crljen and D. C. Langreth, Phys. Rev. B **35**, 4224 (1987).
[8] K. Burke, D. C. Langreth, Z. Y. Zhang, and M. Persson, Phys. Rev. B **47**, 15 (1993).
[9] M. Head-Gordon and J. C. Tully, J. Chem. Phys. **96**, 3939 (1992).
[10] M. Head-Gordon and J. C. Tully, Phys. Rev. B **46**, 1853 (1992).
[11] J. C. Tully and M. Gomez, J. Vac. Sci. Technol. A **11**, 1914 (1993).
[12] R. Brako and W. Brenig, Surf. Sci. **336**, 27 (1995).
[13] D. C. Langreth and M. Persson, in *Laser Spectroscopy and Photochemistry on Metal Surfaces*, edited by H.-L. Dai and W. Ho (World Scientific, River Edge, NJ, 1995).
[14] C. T. Rettner, F. Fabre, J. Kimman, and D. J. Auerbach, Phys. Rev. Lett. **55**, 1904 (1985).
[15] C. T. Rettner *et al.*, Surf. Sci. **192**, 107 (1987).
[16] A. Groß and W. Brenig, Chem. Phys. **177**, 497 (1993).
[17] G. A. Gates, G. R. Darling, and S. Holloway, J. Chem. Phys. **101**, 6281 (1994).
[18] J. R. Prybyla *et al.*, Phys. Rev. Lett. **64**, 1537 (1990).
[19] J. A. Prybyla, H. W. K. Tom, and G. D. Aumiller, Phys. Rev. Lett. **68**, 503 (1992).
[20] R. R. Cavanagh, D. S. King, J. C. Stephenson, and T. F. Heinz, J. Phys. Chem. **97**, 786 (1993).
[21] M. Morin, N. J. Levinos, and A. L. Harris, J. Chem. Phys **96**, 3950 (1992).
[22] C. J. Hirschmugl, G. P. Williams, F. M. Hoffman, and Y. Chabal, Phys. Rev. Lett. **65**, 480 (1990).
[23] E. R. Behringer *et al.*, Nucl. Instrum. Methods Phys. Res. Sect. B **78**, 3 (1993).
[24] G. A. Kimmel, D. M. Goodstein, Z. H. Levine, and B. H. Cooper, Phys. Rev. B **43**, 9403 (1991).
[25] G. A. Kimmel, D. M. Goodstein, and B. H. Cooper, J. Vac. Sci. Technol. A **7**, 2186 (1989).
[26] D. M. Newns, T. F. Heinz, and J. A. Misewich, Prog. Theor. Phys. Suppl. **106**, 411 (1991).
[27] J. A. Misewich, T. F. Heinz, and D. M. Newns, Phys, Rev. Lett. **68**, 3737 (1992).
[28] B. Fain, H. L. S, J. Grotemeyer, and E. W. Schlag, Chem. Phys. Lett. **202**, 357 (1993).
[29] P. W. Anderson, Phys. Rev. **124**, 41 (1961).
[30] D. M. Newns, Phys. Rev. **178**, 1123 (1969).
[31] R. Brako and D. M. Newns, Solid State Commun. **55**, 633 (1985).
[32] H. Kasai and A. Okiji, Surf. Sci. **183**, 147 (1987).
[33] J. B. Marston, D. R. Andersson, E. R. Behringer, and B. H. Cooper, Phys. Rev. B **48**, 7809 (1993).
[34] D. C. Langreth and P. Nordlander, Phys. Rev. B **43**, 2541 (1991).
[35] H. Keiter and J. C. Kimball, Int. J. Magn. **1**, 233 (1971).
[36] F. C. Zhang and T. K. Lee, Phys. Rev. B **28**, 33 (1983).
[37] Y. Kuramoto, Z. Phys. B **53**, 37 (1983).
[38] N. Grewe, Z. Phys. B **53**, 271 (1983).
[39] P. Coleman, Phys. Rev. B **29**, 3035 (1984).
[40] T. A. Costi, J. Kroha, and P. Wölfle, Phys. Rev. B **53**, 1850 (1996).
[41] L. P. Kadanoff and G. Baym, *Quantum Statistical Mechanics* (Benjamin, New York, 1962).
[42] L. V. Keldysh, Zh. Éksp. Teor. Fiz. **47**, 1515 (1964) [Sov. Phys. JETP **20**, 1018 (1965)].
[43] H. Shao, D. C. Langreth, and P. Nordlander, Phys. Rev. B **49**, 13 929 (1994).
[44] A. Yoshimori, Surf. Sci. **342**, L1101 (1995).
[45] M. Head-Gordon and J. C. Tully, J. Chem. Phys. **103**, 10 137 (1995).
[46] C. Springer, M. Head-Gordon, and J. C. Tully, Surf. Sci. Lett. **320**, L57 (1994).
[47] H. Shao, D. C. Langreth, and P. Nordlander, Phys. Rev. Lett. **77**, 948 (1996).
[48] T. Brunner, D. C. Langreth, P. Nordlander, and H. Shao, in *Proceedings of the 18th Taniguchi Symposium*, edited by A. Okiji, H. Kasai, and K. Makoshi (Springer, Berlin, 1996).
[49] S. Hershfield, J. H. Davies, and J. W. Wilkins, Phys. Rev. Lett. **67**, 3720 (1991).
[50] S. Hershfield, J. H. Davies, and J. W. Wilkins, Phys. Rev. B **46**, 7046 (1992).
[51] Y. Meir, N. S. Wingreen, and P. A. Lee, Phys. Rev. Lett. **70**, 2601 (1993).
[52] T. K. Ng, Phys. Rev. Lett. **23**, 3635 (1993).
[53] N. S. Wingreen and Y. Meir, Phys. Rev. B **49**, 11 040 (1994).
[54] A.-P. Jauho, N. S. Wingreen, and Y. Meir, Phys. Rev. B **50**, 5528 (1994).
[55] D. C. Ralph and R. A. Buhrman, Phys. Rev. Lett. **72**, 3401 (1994).
[56] H. Kojima, Y. Kuramoto, and M. Tachiki, Z. Phys. B **54**, 293 (1984).
[57] E. Müller-Hartmann, J. Magn. Magn. Mater. **57**, 281 (1984).
[58] Y. Kuramoto and H. Kojima, Z. Phys. B **57**, 95 (1984).
[59] Y. Kuramoto and E. Müller-Hartmann, J. Magn. Magn. Mater. **52**, 122 (1985).
[60] S. Maekawa, S. Takahashi, S. Kashiba, and M. Tachiki, J. Phys. Soc. Jpn. **54**, 1955 (1985).
[61] N. E. Bickers, D. L. Cox, and J. W. Wilkins, Phys. Rev. B **36**, 2036 (1987).
[62] N. E. Bickers, Rev. Mod. Phys. **59**, 845 (1987).
[63] A. C. Hewson, *The Kondo Problem to Heavy Fermions* (Cambridge University Press, Cambridge, 1993).
[64] P. Coleman, Phys. Rev. B **35**, 5072 (1987).
[65] P. Coleman and N. Andrei, J. Phys. C **19**, 3211 (1986).
[66] B. Jin, T. Matsuura, and Y. Kuroda, J. Phys. Soc. Jpn. **60**, 580 (1991); Y. Kuroda, Y. Ono, K. Miura, B. Jin, H. Jichu, D. S. Hirashima, and T. Matsuura, Prog. Theor. Phys. Suppl. **108**, 173 (1992).
[67] D. C. Langreth, in *Linear and Nonlinear Electron Transport in Solids*, edited by J. T. Devreese and V. E. van Doren (Plenum, New York, 1976).
[68] D. C. Langreth, Phys. Rev. **150**, 516 (1966).
[69] A. Blandin, A. Nourtier, and D. Hone, J. Phys. (Paris) **37**, 369 (1976).
[70] A. Nourtier, J. Phys. (Paris) **38**, 579 (1977).
[71] P. Schlottmann, in *Valence Fluctuations in Solids*, edited by L. M. Falicov, W. Hanke, and M. B. Maple (North-Holland, Amsterdam, 1981).
[72] Y. Kuramoto and H. Kojima, J. Magn. Magn. Mater. **47/48**, 329 (1985).

[73] The perceptive reader will also notice a very slight upturn in the curves as the temperature is lowered below ~ 0.03. This is an artifact caused by the fact that the NCA begins to break down at this temperature in the mixed valent regime.

[74] H. Shiba, J. Phys. C **15**, 5421 (1975).
[75] A. Yoshimori and A. Zawadowski, J. Phys. C **15**, 5241 (1982).
[76] Houghton, N. Read, and H. Won, Phys. Rev. B **35**, 5123 (1987).